Dynamic Moire Interferometry Investigations of Elastic Wave Propagation in ASTM A-710 IZOD Specimens

J. S. EPSTEIN*, V. A. DEASON** and W. G. REUTER**

*The Center for the Advancement of Computational Mechanics, The Georgia Institute of Technology, Atlanta, G.A., 30332, USA

**Applied Optics Group, Fracture and Dynamic Behavior Group, respectively The Idaho National Engineering Laboratory, Idaho Falls, ID 83415, USA

ABSTRACT

An investigation on the elastic wave propagation displacement fields in an Izod specimen fabricated from ASTM A-710 steel has been conducted. The principal tool for this investigation is dynamic moire interferometry. The method of dynamic moire interferometry will be outlined relative to crack tip phenomena. A near tip dynamic stress intensity factor algorithm will be outlined with relevance to the mixed mode dynamic moire interferometry displacement data. This paper will concentrate on experimental methods. Mode I stress intensity factors will be extracted from the U displacement fields. Conclusions will be drawn on the degree of Izod specimen inertia effects relative to mode I loading with a fatigue pre-crack instead of the typical 45 degree notch.

KEYWORDS

Dynamic Fracture, Dynamic Moire Interferometry, IZOD Specimen, Pulsed Ruby Laser

INTRODUCTION

Many methods exist to determine the dynamic elastic stress intensity factor as a function of time. The two most routinely used techniques are dynamic photoelasticity and the method of caustics. Extensive review articles, with relevance to cracks, have been prepared by Dally [1979], Burger [1987] and Kalthoff [1987] on dynamic photoelasticity and caustics respectively. While dynamic photoelasticity is a full field technique describing the stress field surrounding a crack tip; the method is limited to a well defined class of materials exhibiting birefringence effects, and whose equation of state is clearly defined relative to the birefringence of the material. The method of caustics, relying on local refractive index changes through transparent materials or mirror effects from out of plane crack tip dimpling on opaque materials is not a full field technique. The contraction produces a caustic or lack of information region on the focal plane of the imaging lens system. For crack tip regions, the caustic method is a one-parameter stress intensity factor extraction whose full understanding of three dimensional lateral expansion effects is currently under active research. The fundamental quantity by which both techniques produce information is displacement, in transparent materials for two dimensional photoelasticity, the displacement induced birefringence information is averaged through the thickness, in opaque materials, for the method of caustics, an assumed two dimensional in-plane displacement produces an out of plane contraction.

If displacement is the desired quantity then moire methods or image correlation techniques can be more appropriate. It should be noted that these methods are surface sampling. Techniques such as neutron diffraction and synchrotron radiation diffraction offer the promising ability for detailed interior displacement investigations even in the time domain [1985]. Optically processed image correlation through speckle was performed dynamically by Crostack [1985]. Jolles and Peters are using digitally processed image correlation combined with high speed video to process displacement information [1986].

The amplitude moire methods may be used to study the in-plane free surface displacements. Using amplitude moire methods, Kobayashi [1967], studied transient fracture in magnesium. The moire methods produce displacement information from an ordered pattern which results in excellent clarity in displacement detail, in a full field fashion. The major problem encountered with the classical moire methods is spatial resolution. Due to diffraction effects, the surface sampling grating cannot exceed 40 l/mm. The implication then is that the smallest spatial region that can be sampled is the inverse of the grating frequency. With 40 l/mm gratings the surface detail resolution is 25 microns. The ability to interpolate displacement information can exceed the frequency of the surface grating with multiplication techniques. With 40 l/mm surface gratings the basic deformation processing sensitivity is 25 microns. The deformation processing resolution can be extended to 12 microns with multiplications of two. The result of classical moire applied to small deformation fracture problems is a lack of spatial detail and displacement processing resolution.

Dynamic moire interferometry has the ability to produce surface displacement fields in the time domain with excellent spatial detail and displacement processing resolution with an adequate time sampling for structural problems involving high compliance materials. Developed two years ago by Deason [1985], dynamic moire interferometry is now producing highly detailed maps of surface displacement indicative of the microstructure and adequate for localized dynamic stress intensity factor determination in structural materials. The next section will describe the principals of dynamic moire interferometry.

STATIC DYNAMIC MOIRE INTERFEROMETRY

Diffraction Grating Moire

To improve the sensitivity of the moire method, Professor D. Post and associates at Virginia Polytechnic Institute (VPI) perfected a different technique, called diffraction moire by analogy with amplitude type moire. This method is actually a form of diffraction grating interferometry. This technique also produces full field data, but with an ultimate displacement resolution of 0.2 microns per fringe. The method consists of bonding a diffraction grating intimately to a surface under study (Figure 1). The grating is illuminated by two mutually coherent laser beams oriented such that the respective first order diffraction beams leave the grating coaxially and normal to the plane of the grating (Figure 2). If the grating is undistorted and the incident beams are well collimated, the two first order beams interfere to give a single broad fringe. Any deviation from perfect alignment or a distortion in the grating will cause the exit beams to diverge either uniformly, producing a set of parallel interference fringes, or locally, producing a local region where fringes appear. A review article by Post [1987] has thoroughly described this technique both theoretically and practically, and has confirmed the excellent quality of the resulting data. Livnat and Post [1985] have also shown the correspondence between the mathematical description of classical (coarse) moire and diffraction moire.

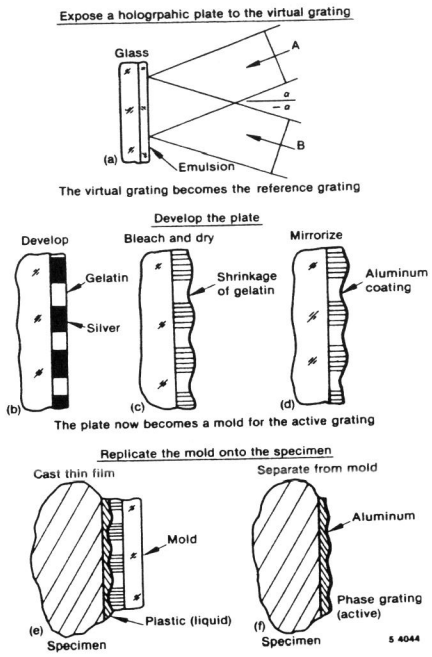

Figure 1. The replication of a phase diffraction grating to the specimen surface.

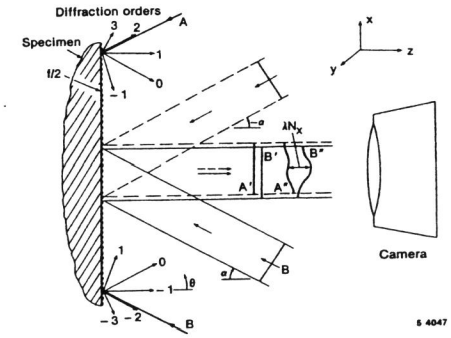

Figure 2. Two beam interferometry with a diffraction grating.

DYNAMIC MOIRE INTERFEROMETRY

The purpose of this paper is to present results of efforts to extend the technique of diffraction moire interferometry to the study of rapidly changing stress fields, especially as they interact with material texture, structure, or defects such as cracks. In particular, the technique has been applied to the study of a composite material response to impulsive loads (Deason [1987]) and in this paper, cracks under impulsive loading. The approach was to substitute a pulsed ruby laser for the CW lasers normally used and to rely on the high power (0.5 J) and short pulse width (20 ns) to sample stress wave-induced material motion. Various problems peculiar to the technique were encountered and the solutions were described in detail in an earlier paper (Deason [1987]).

Equipment

The cameras:

A Beckman and Whitley model 195 turbine-driven rotating mirror streak camera without slits was used to record multipulse sequences on 35-mm film strips. A press camera with focal plane shutter was used to record single and double exposure interferograms on 4x5-inch film sheets. In all cases, Kodak High Speed Infrared film was used whose spectral sensitivity is optimized to the wavelength of the pulsed ruby laser. The film can resolve approximately 40 l/mm.

The pulsed ruby laser:

The laser used in these studies was an Apollo 22HD double pulsed holographic ruby laser. The pulse width was a few tens of nanoseconds and the pulse energy was typically about 0.5 J. The oscillator cavity consisted of a rear 100% mirror and a front water cooled etalon/output coupler. Internal to the cavity were an acousto-optic Q-switch, a 76.2 mm long x 9.5 mm helical flash lamp pumped ruby rod, and a 1.78-mm diameter transverse mode selector. Exterior to the cavity were a 152 mm long x 9.5 mm ruby rod amplifier and various dielectric turning mirrors. The laser operated at 694.3 nm in the TEM_{oo} mode with a coherence length of several meters. The output beam was expanded by a negative lens and collimated by a 914 mm focal length, 152-mm diameter air-spaced astronomical doublet to provide the 152-mm diameter beam used throughout the dynamic studies. Careful attention was paid to reducing stray scattered light. The laser has been extensively modified to permit controlled multiple pulses at rates from 25,000 to 110,000 pulses per second. Each pulse is about 20 ns long with nearly 40 mJ energy. Up to 40 pulses can be produced in a given sequence with full control over the pulse timing. Figure 3 shows a typical Q-switch command sequence and the resultant laser pulses. An occasional pulse is missed or doubled.

Problems peculiar to the use of the ruby laser:

The output of a pulsed ruby laser is so brief, bright, and infrequent (20 ns, > 100 MW/cm^2, one or two pulses per min) that one usually uses a CW HeNe laser to align optics and show where the illumination falls on the specimen. This poses little problem for normal types of reflective or refractive optics since the wavelength of the HeNe laser (632.8 nm) is close to that of the ruby (694.3 nm). However, when diffractive optical elements are used, the HeNe and ruby light become separated and are no longer coaxial. In the present application, this introduces a fringe pattern with fringe density equal to about 10% of the grating groove density, or about 200 fringes per mm.

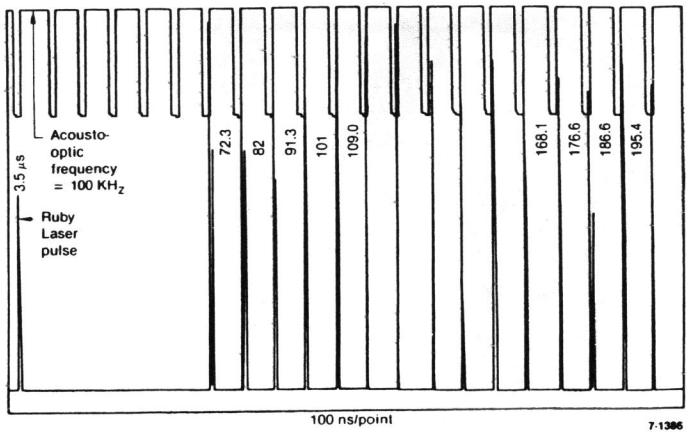

Figure 3. Multi-pulsing of the ruby laser with an acousto-optic modulator.

When the holographic gratings are made for replication onto the specimen, a dual grating system is created, one for the HeNe laser and one for the ruby. The relationship between the two is carefully controlled to assure mutual alignment. During testing, the HeNe grating is used with a HeNe laser to align the system, and the ruby grating and ruby laser are used to take data. Registration of the gratings during manufacture ensures common alignment of the HeNe and ruby laser moire patterns during a test. The production of these gratings has been described elsewhere (Deason [1987]). Recently, dual superimposed Ruby/HeNe gratings have been produced. These gratings will alleviate the separate nature of the current dual Ruby/HeNe gratings, permitting static optical alignment via the HeNe portion over the data portion of the specimen grating.

SPECIMEN

The specimen configuration is a modified ASTM E-23 Izod specimen. The Izod Specimen was chosen due to a discussion by Curran [1983] in comparing the different notched specimens to elastic impact. Curran noted that the Izod unlike the Charpy specimen, yields a long term mode I dominant loading. The specimen under study is a modified Izod specimen shown in Figure 4. The specimen is 100 mm long, 24 mm wide and 12 mm in thickness with a fatigue pre-crack in the center of the length direction. The fatigue pre-crack extends 12 mm into the specimen width. The material chosen for testing was an ASTM A-710 steel; a fairly ductile steel with a yield stress of 479 MPa, an ultimate stress of 635 MPa and a strain hardening exponent of 10. The modification was chosen as a matter of convenience so as to only study specimen loading under strong elastic impact and not crack initiation. The modified geometry of ASTM A-710 Izod specimen was felt by prejudgment to offer such a compromise.

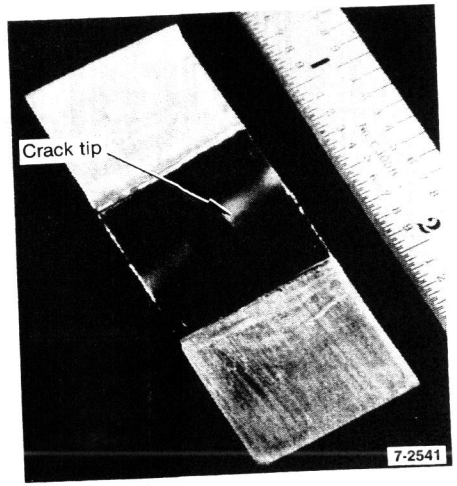

Figure 4. Modified Izod specimen of ASTM A-710 (scale in.).

DYNAMIC LOADING

A solenoid valve-operated pneumatically-driven piston accelerates a steel bar. This steel bar in turn impacts a miniature Hopkinson bar in contact with the specimen. The conical tup of the bar is removable so that it can be machined of the same material as the Izod specimen to minimize impedance mismatch. The miniature Hopkinson bar configuration is shown in Figure 5 with a Charpy impact specimen in the loading fixture instead of the modified Izod specimen. The concept of a miniature Hopkinson bar at first seems illogical as the principal of the Hopkinson bar is a relatively long bar to smooth out waveguiding reflections and dispersion so that a long time length quasi one dimensional wave impacts the specimen. A novel approach was taken with the miniature bar. In this case the diameter is small, 12 mm so that a typical impact wave of approximately 70 microseconds will yield nearly bulk wave travel in the bar. The Hopkinson bar used in this study is one in reflection which was studied in detail by Mines [1985]. Two Micro-Measurement EP-06-062AK-120 gages were applied to the bar. The two gages were located 57.6 and 117.2 mm from the conical tup. As noted by Mines [1985], the conical tup is considered to have minimal effect to the input and return wave front.

TEST PROCEDURES

Electro-mechanical Arrangement

The Izod specimens were securely fastened in the massive mounting bracket, Figure 5. The Hopkinson bar tup was positioned firmly against the Izod specimen. Besides strain gages, the tup was instrumented to sense electrical contact between the sliding impact bar and the Hopkinson bar. Covers were placed over the Hopkinson bar to protect the strain gages from spurious noise due to high amplifications (2000x). The gages were also shielded with coaxial cables. An overall view of the experimental arrangement is shown in Figure 6 and again in the schematic of Figure 7. During use, the impactor bar slides forward in a Teflon sleeve after separating from the pneumatic piston; it then strikes the Hopkinson bar . At the moment of impact, electrical contact between the impactor and the bar is used to signal the start of an event. All subsequent timing is referenced to this time zero. Prior to contact, an earlier timing mark is created when a pin on the sliding impact bar passes through and obstructs a laser beam from a 5-mW laser. The interruption of this beam generates a TTL signal used to initiate the ruby laser firing sequence which requires several hundred microseconds and which must therefore begin before impact. Timing and laser control were performed by a custom built four-channel delay generator with a 10-MHz clock.

The specimen is lightly impacted once before measurement to record data from an acoustic transducer (5 MHz) located on the crack tip opposite the grating surface. Details of this signal are used to establish timing delays for the laser pulses.

Optics

The specimen grating is illuminated by either of two collinear laser beams, one from a 10 mW HeNe alignment laser and the other from a ruby laser. Each laser beam is divided into two beams which illuminate the specimen grating at an angle appropriate to create the diffraction moire data. The HeNe beams are used to align the optics relative to the grating, and the data are recorded using the ruby laser. Mirrors with 1/10 wave surfaces were used throughout.

The gratings were crossed, that is, with two superimposed 1200 lines/mm gratings whose groove directions were at 90 degrees to each other. This allows one to simultaneously record both X and Y displacement fields from the specimen. Unfortunately, only the X-displacement field was recorded. Thus, the grating grooves used were those which were perpendicular to the crack face. The optical design utilizing a multiplication of 2 provides an equivalent sensitivity of 1/2400 mm of in-plane displacement per interference fringe.

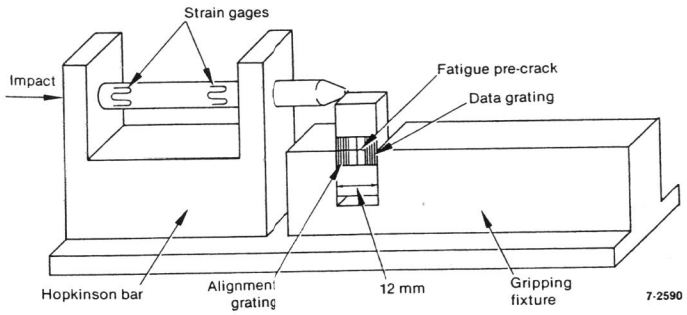

Figure 5. Miniature Hopkinson bar assembly with Izod specimen holder.

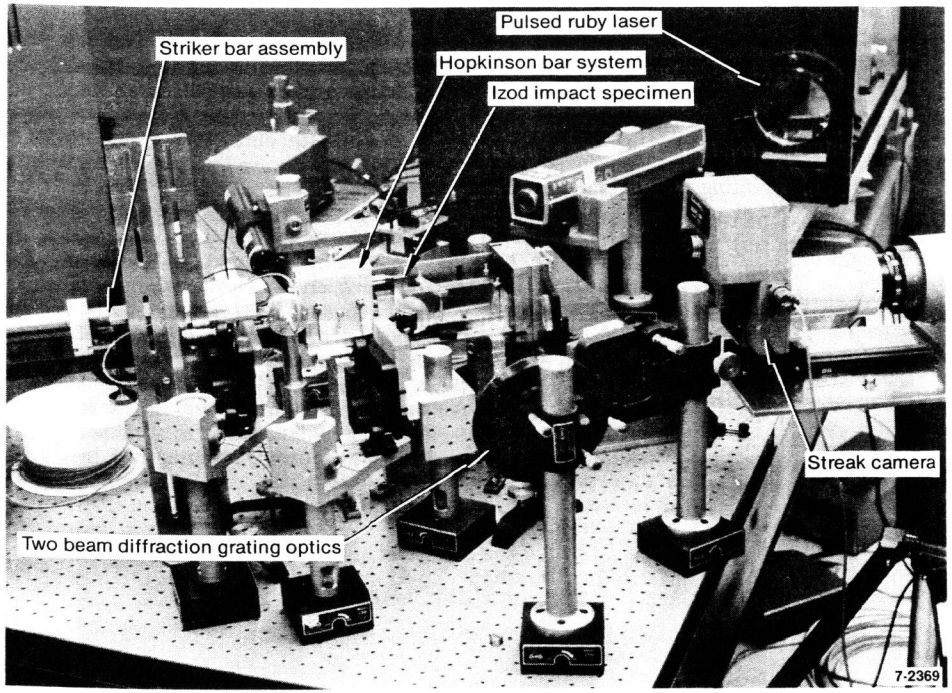

Figure 6. Overall system view of the optical and mechanical test set up.

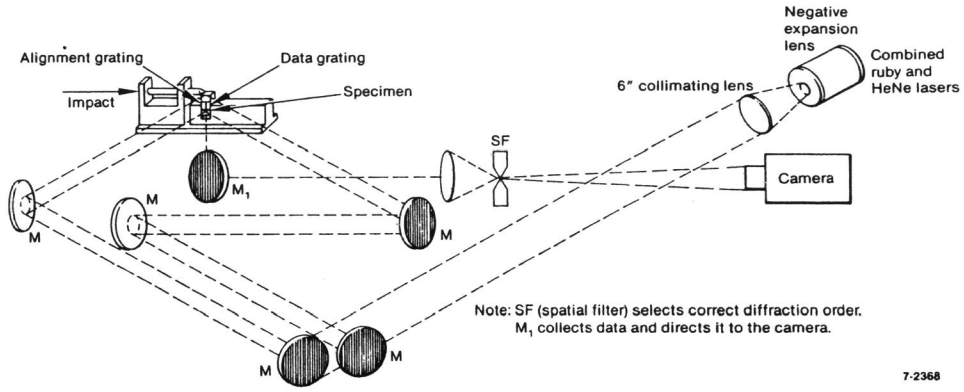

Figure 7. Schematic of the test set up with an Izod specimen and holder.

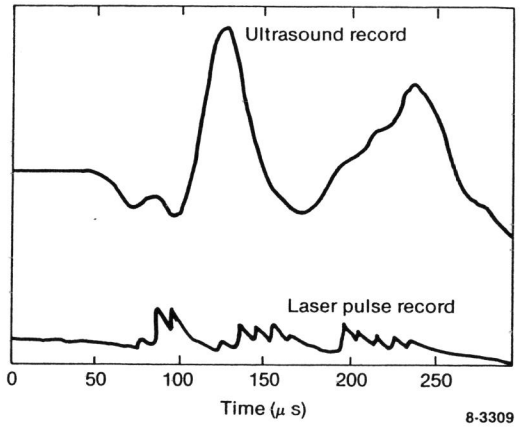

Figure 8. Laser pulsing output with piezoelectric sensor record.

Data: Single Interferogram

During the testing, records of specimen deformation in the form of diffraction moire interferogram were recorded in two formats. The first type of recording was a double exposed interferogram on 4 x 5-in. film. The first exposure was of the unloaded specimen and included a 5 lines/mm carrier pattern used to permit certain spatial filtering techniques during data reduction. The second exposure was of the specimen under load, also with the carrier pattern. The timing of the second exposure could be varied to observe deformation during any desired part of the loading event. Only a single interferogram was made during each loading event. This format has the advantage of optically removing any preload distortions present in the specimen. Its major disadvantage is that the specimen displacement field is only recorded at a single instant in time.

Data: Multiple Interferogram

A second type of recording was used for the first time during these tests. This consisted of data generated by multiple pulses of the ruby laser during a single event. The data were recorded as a series of interferogram on a strip of Kodak 35 mm Infrared film in the turbine-driven, rotating mirror streak camera. No slit was used, so a full image was present on the film at all times. We relied on the short pulse length of the ruby laser to record blur-free interferogram on the film. The mirror in the camera was rotating at a nominal 1000 rps during most of the tests. A major problem with the turbine tests was static electricity forming on the film surface during loading in the circular drum.

Testing Sequence:

The typical sequence of events is detailed as follows: the pulsed laser capacitance banks are charged. The room lights are turned out. In order to activate the streak camera turbine, a electro-mechanical shutter and helium solenoid valve must be opened. This activation in turn triggers a 30 second timer. The timer will shut the helium solenoid in turn shutting down the camera turbine after 30 seconds. The timer is a safety item as once the turbine is brought to speed at up to 1000 revolutions per second, a potential exists to ruin the turbine components from too long a run period. From experience it has been found that 30 seconds is a safe period in which to leave the turbine running. When the turbine is brought up to speed, the air ram is activated which in turn accelerates the sliding bar. Before impacting the Hopkinson bar, a trigger laser beam is broken by the sliding bar. This trigger beam in turn discharges the capacitance banks through the laser rod flash lamps which subsequently begins to lase the chromium doped ruby rods. Upon impact, electrical contact is made between the sliding bar and the Hopkinson bar thus beginning the time delay sequence to fire the train of pulses from the ruby rods. The delay sequence is set to capture the impact wave in the specimen. This delay sequence is found from pre-hitting the Izod specimen and recording the time signal from the piezoelectric sensor. After the laser firing the turbine is slowly brought down from speed. The film is removed from the drum. The room lights are turned on.

Two major problems existed during this series of tests. First, the impact process is extremely detailed with little room for error. A typical test required two persons to conduct, each with a check list, one person to control the streak camera turbine and one person to fire the air ram. Second, the streak camera was made in 1952. The mirror surface was abraded after years of use. Further, the turbine leaked oil onto the mirror. This leakage required turbine removal after 2 -3 tests and careful cleaning, a time consuming and tedious process.

An alternative is to use an electro-optic image converter camera with a broad pulsed laser. The current problem with these cameras is there small image size and resolution at 7 line pairs per mm.

Figure 8 shows a typical laser pulsing output with the acoustic record superimposed.

RESULTS

Figures 9 and 10 detail the strain gage response signals from the Hopkinson bar. The pulse width delivered by the striker bar is 74 μs. Following the method outlined by Mines, [1985], it was determined that the impact pulse delivered a peak amplitude of 17.46 MPa after approximately 22 μs. In retrospect, a longer striker bar would have been more appropriate due to the relatively short input pulse length (74 μs) delivered by the current striker bar. Figure 11 details a time sequenced displacement field of displacements normal to the crack tip. This pattern contains a constant rotational mismatch. The mismatch was a result of a loose optic where the impact wave reached the optic before the diffraction grating. The mismatch pattern is constant throughout the deformation process and can be subtracted to obtain the actual data. Two important trends appear in the data. First the initial wave loading of the specimen is fairly symmetric. However, wave reflections in the specimen lead to a highly asymmetric displacement pattern surrounding the crack tip. This displacement field confirms the results of Curran [1983]. Although symmetry is found in the initial loading confirming Curran's results; dissymmetry is found in later loading from multiple wave reflections. Thus the Izod specimen can be one of minimal specimen inertia contributing to mode I type dynamic fracture if crack initiation occurs during early loading. However, the Izod specimen can have large mixed mode specimen inertia effects if initiation occurs later in time. Typically, the loading of the specimen is with a massive swinging pendulum. Depending on the material under test, the pendulum may not carry enough momentum to initiate fracture during early time of contact. Rather the undesired effect of later initiation due to sustained long time contact of the pendulum with the specimen may occur, resulting in a highly inertia coupled mixed mode form of initiation.

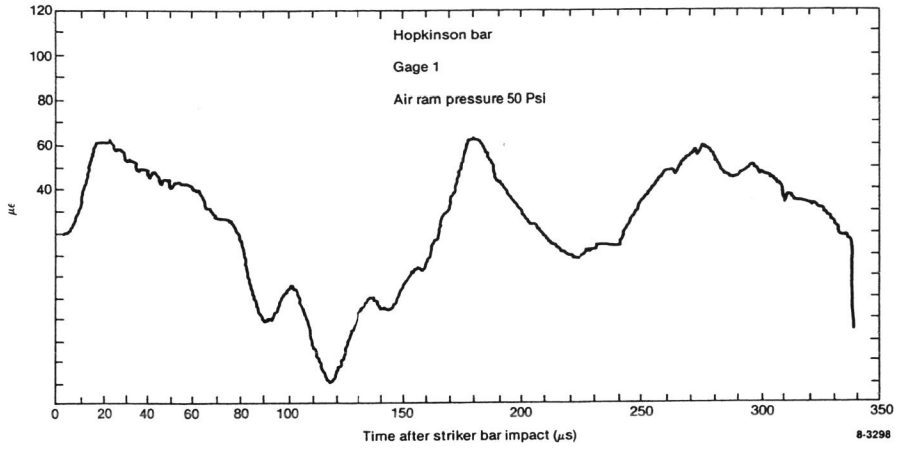

Figure 9. Strain verses time history for gage 1 of the Hopkinson Bar.

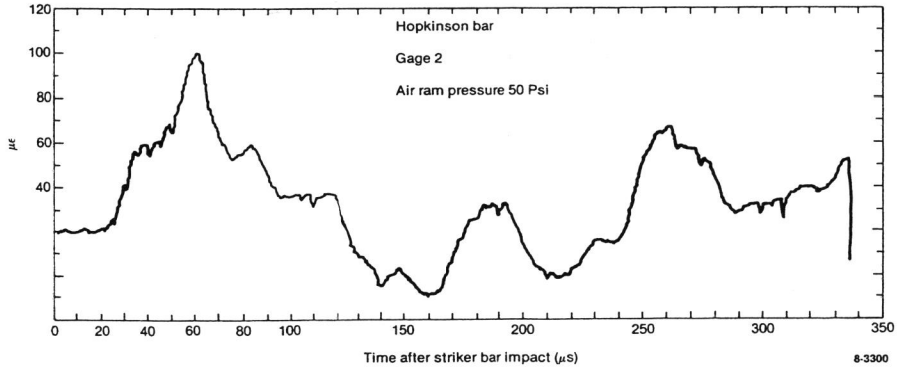

Figure 10. Strain verses time history for gage 2 of the Hopkinson Bar.

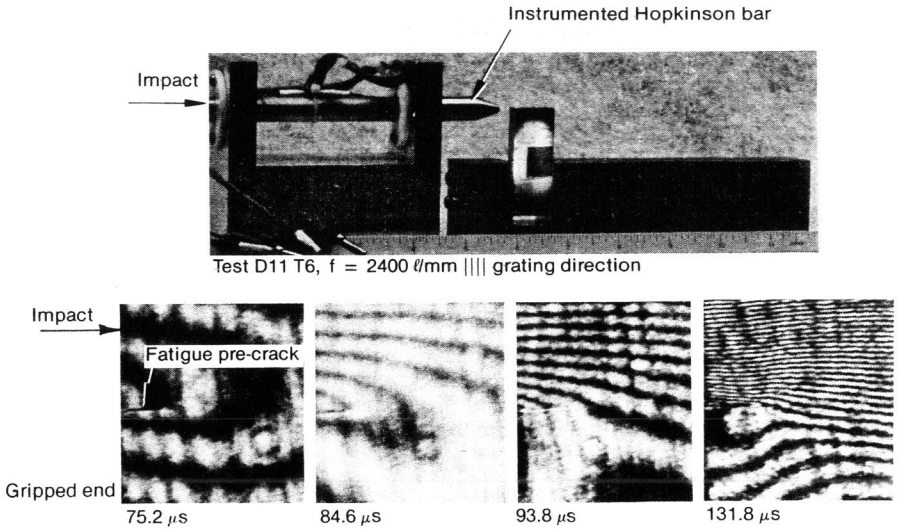

Figure 11. Time sequenced U (normal to crack plane) displacement fields, the grating frequency is 2400 l/mm the impact pressure is 7.85 Mpa.

STRESS INTENSITY FACTOR DETERMINATION FOR A STATIONARY CRACK:

Kobayashi [1978] noted that for a stationary crack under dynamic loading the form of eigenfunction displacement relationships in the U (normal to the crack tip) and V (in the opening mode of the crack tip) fields reduced to the classical Williams [1957] form. If one is local to a crack tip such that the lowest eigenvalue dominans the solution, typically referred to as a "robust" parameter, one may truncate the asymptotic crack tip solution as follows:

$$U = (K_I/\mu)(r/2\pi)^{1/2}F_1(\theta) + (K_{II}/\mu)(r/2\pi)^{1/2}F_2(\theta) + U^\circ \qquad (1)$$

where: $F_1(\theta) = \cos(\theta/2)[1/2(k-1)+\sin^2(\theta/2)]$,
$F_2(\theta) = \sin(\theta/2)[1/2(k+1)+\cos^2(\theta/2)]$

and

$$V = (K_I/\mu)(r/2\pi)^{1/2}H_1(\theta) + (K_{II}/\mu)(r/2\pi)^{1/2}H_2(\theta) + V^\circ \qquad (2)$$

where: $H_1(\theta) = \sin(\theta/2)[1/2(k+1)-\cos^2(\theta/2)]$,
$H_2(\theta) = \cos(\theta/2)[1/2(k-1)+\sin^2(\theta/2)]$

where: μ is the shear modulus,
k is (3-4n) for plane stress and,
k is (3-n)/(1+n) for plane strain,
U°, V° are higher order non - singular far field terms.

A procedure is then outlined for determining near field mix mode stress intensity factors from either the U or V fields utilizing moire interferometry displacement data. Consider the U displacement field ahead of the crack tip evaluated at 0 degrees:

$$U = (K_I/\mu)(r/2\pi)^{1/2}F_1(\theta) + U^\circ \tag{3}$$

rearrangement of (3) yields:

$$K_{ap} = U(\mu)(r/2\pi a)^{-1/2}(F_1(\theta))^{-1}$$

$$= K_I + U^\circ(\mu)(r/2\pi a)^{-1/2}(F_1(\theta))^{-1} \tag{4}$$

where: a is the crack size.

Plotting K_{ap} verses $(r/a)^{1/2}$ will yield a linear relationship only in the zone where the first eigenvalue or K_I dominates, local to the crack tip. Extrapolating the asymptotic solution (3) to the origin yields K_I. With K_I determined, one may evaluate (1) at 90 degrees or (2) at 0 degrees and perform the same procedure of extrapolation through the linear zone to extract K_{II}.

Figures 12, 13, and 14 detail log(U) verses log(r) plots of the displacement data taken at 0 degrees to the crack tip. The 0 degree data line was chosen in order to eliminate cross derivatives (or rotation) of the U displacements that would be found when taking data at 90 degrees. As can be seen from these figures, the slope of the curves yields the first displacement eigenvalue λ:

$$U = Ar^{\lambda}f(\theta) \tag{5}$$

$$\log(U) = \lambda\log(r) + \log(A) + \log(f(\theta)) \tag{6}$$

The slope found from these figures is close to the theoretical values of 0.5. Possible reasons for the slope not perfectly agreeing with the theoretical value may lie with the determination of the fringe centers. The two parameter method outlined was then applied within this singularity dominant zone to yield the mode I dynamic stress intensity factor as shown in figure 15.

Figure 16 details the dynamic stress intensity verses time for the impact of the Izod specimen. It should be noted that the curve only details the mode I stress intensity values from a highly mixed mode condition as evidenced by the high degree of dissymetry in the displacement fields of figure 11.

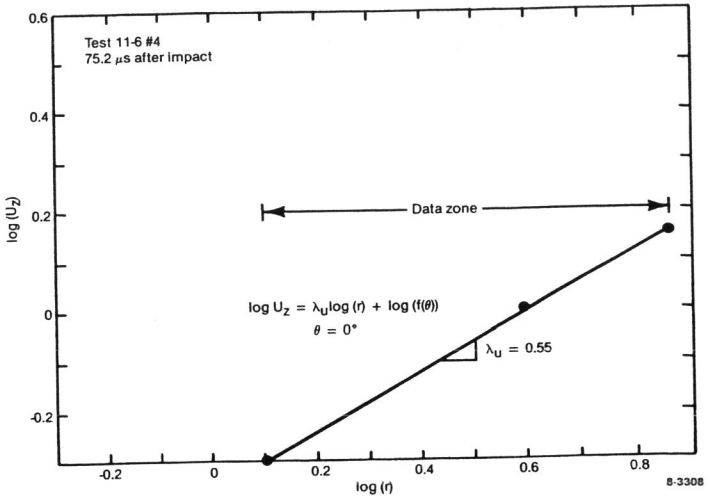

Figure 12. Log(U) verses Log(r) for 75 microseconds after impact.

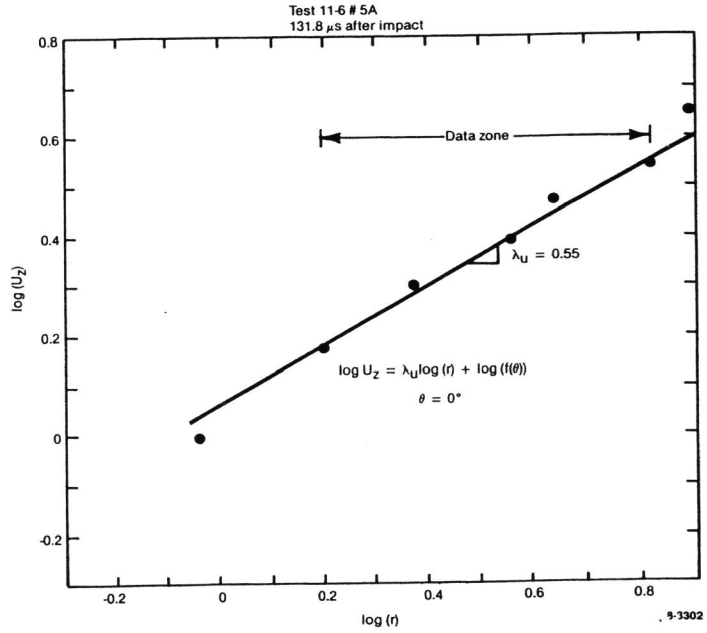

Figure 13. Log(U) verses Log(r) for 131 microseconds after impact.

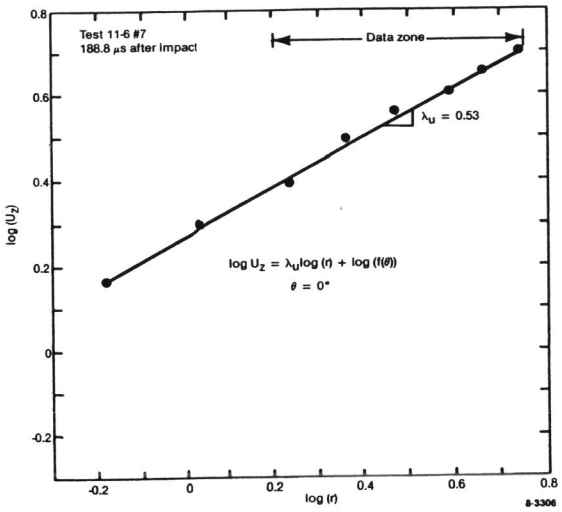

Figure 14. Log(U) verses Log(r) for 188 microseconds after impact.

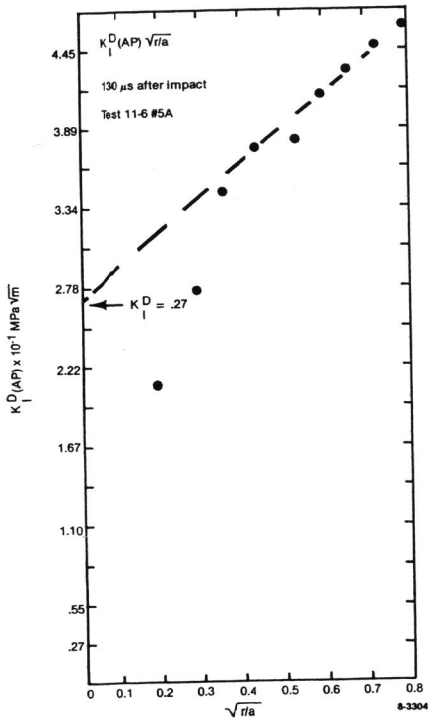

Figure 15. A plot of the apparent mode I dynamic stress intensity factor verses $(r/a)^{1/2}$.

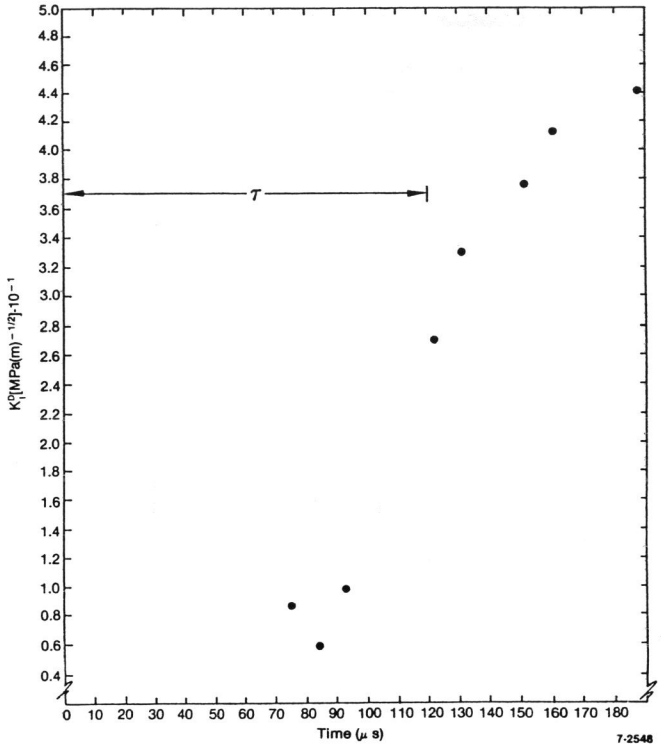

Figure 16. The mode I dynamic stress intensity verses time after impact for the Izod specimen.

CONCLUSION

An experimental method has been utilized to extract near field elastic displacement fields of cracked bodies under stress wave loading with high spatial resolution and sub-micron displacement sensitivity. The method developed combines pulsed lasers with diffraction grating moire. A novel miniature Hopkinson bar has been developed for small optics type tests. Transient displacement fields in an Izod specimen fabricated from ASTM A-710 steel have been produced with a sensitivity of 0.4 microns to in-plane displacement normal to the crack front. It has been found that during initial time scales symmetric loading occurs on the crack. However during later time scales unsymmetric loading occurs. The early time loading confirms the work of Curran [1983]. The later time scale information is novel with implications on the manor in which dynamic initiation can occur with swinging pendulum tests for ductile Izod specimens. It is possible that for tough materials, where the pendulum lacks energy to initially fracture the specimen, mixed mode loading will occur with specimen inertia effects - a highly undesirable situation. A method of data extraction has been outlined with particular relevance to the near field data that dynamic moire interferometry produces. This method relies on the local nature of the asymptotic elastic solution for stationary cracks under dynamic loading. Mode I dynamic stress intensity factors were subsequently extracted. Future work will concentrate on an extraction of mode II dynamic stress intensity factors from the V field. A comparison will also be sought between this local crack tip asymptotic technique and a method relying on additional higher order non-asymptotic terms in the displacement eigenfunction expansion. A continuum finite element method is currently being pursued for comparison of the data presented.

ACKNOWLEDGMENTS

This work supported by the Office of Naval Research, Dr. Y. Rajapakse program manager and the Department of Energy Office of Basic Energy Sciences, Dr. O.A. Manley program manager under DOE Contract No. DE-AC07-76ID01570. The assistance of Mr. J. Alexander, Mr. S. Lee and Mr. N. Holmes is gratefully acknowledged.

BIBLIOGRAPHY

Allen, A.J., Hutchings, M.T., Windsor, C.G. and Andreani, C., (1985), "Neutron Diffraction Methods for the Study of Residual Stress Fields", Advances in Physics, vol. 34, no. 4, pp. 445-473.

Burger, C.,(1987), "Photoelasticity", Handbook on Experimental Mechanics, ch.4., A. Kobayashi ed., SEM.

Crostack, H.A., Kruger, A.,(1985), "Measuring Dynamic Stress Distributions by Laser Speckle Techniques", Proceedings, 11th World Conf. on Non-Destructive Testing, pp.636-642.

Curran, R.S.J., Mines, R.A.W. and Ruiz, C.,(1983) "Elastic Impact Loading of Notched Beams and Bars", Int. J. Frac., pp. 129-14.

Dally, J.W., (1979), "Dynamic Photoelastic Studies of Fracture", Exp. Mech., vol. 19, pp. 349-367.

Deason, V., Epstein, J. and Reuter, W.G., (1985), "A Dynamic Moire Interferometry Technique", Proceedings, 1985 Spring SEM Meeting, pp. 475.

Deason, V.A., and Epstein, J.S., (1987), "Diffraction Moire: The Dynamic Regime", to be published, SPIE O-E LASER 1987.

Kalthoff, J.F., (1987), "Shadow Optical Method of Caustics", Handbook on Experimental Mechanics, ch.9., A. Kobayashi ed., SEM.

Private Discussion, M. Jolles, (1986), Naval Research Laboratory.

Kobayashi, A., D.O. Harris, and W.L. Engstrom, (1967), "Transient Analysis in a Fracturing Magnesium Plate", Exp. Mech., Oct., pp.434-440.

Kobayashi, A., and Mall, S., (1978), "Dynamic Fracture Toughness of Homolite 100", Exp. Mech., vol. 18, no. 1, pp. 11-19.

Livnat, A. and Post, D., (1985), "The Grating Equations for Moire Interferometry and Their Identity to Equations of Geometrical Moire," Experimental Mechanics, vol. 25, no 4, pp. 360-367.

Mines, R.A.W. and Ruiz, C., (1985), "Assessment of Dynamic Methods for the Measurement of Fracture Toughness", Oxford Univ. Report OUEL 1561/85.

Post, D., (1987), "Moire Interferometry", Handbook on Experimental Mechanics, ch 7., A. Kobayashi ed., SEM.

Williams, M.L., (1957), "On the Stress Distribution at the Base of a Stationary Crack", J. Appl. Mech., Trans ASME, vol. 37, Series E (2), pp.409-415.